DOI: https://doi.org/10.3126/forestry.v18i01.41751

Forestry: Journal of Institute of Forestry, Nepal

journal homepage: www.nepjol.info/index.php/forestry

An Assessment on Land Use Land Cover Mapping: Sentinel-2 Versus Landsat-9

Sandesh Dhakal[1*], Saroj Kandel[1], Lila Puri[1], Saurav Shrestha[2]

[1] *Tribhuvan University, Institute of Forestry, Pokhara Campus, Nepal.*
[2] *University of New Haven, USA*

KEYWORDS

LULC
Random forest
Google Earth Engine
Supervised classification
Pokhara

ABSTRACT

Landuse is the human use of land and is inferred from land cover, which refers to the physical and biological cover on the surface of the land. Land use changes and impacts on land cover are key measures of environmental change caused by human activities, especially in rapidly developing areas. Information on such land use change patterns is required for sustainable development planning. Commencement of the Sentinel-2 satellite in mid-2015 and Landsat-9 satellite in late 2021 is opening new possibilities in Earth observation and monitoring through higher spatial, spectral, and temporal resolutions. Many researchers have been curious to compare improvements in these two satellites. This research tests the real difference in the quality of the results delivered by Sentinel-2 and Landsat-9 imagery when basic classification methods are applied. This study aims to assess the precision of the LULC classifications derived from Sentinel-2 and Landsat-9 data and to reveal which dataset presents greater accuracy. The Google Earth Engine (GEE) cloud computing platform was used, and the Pokhara metropolitan area was selected as the study area for this case study. The annual composite of Sentinel-2 Multispectral Instrument (MSI) and Landsat-9 Top-of-Atmosphere (TOA) reflectance, acquired for the period January 1, 2022 to August 31, 2022, was used as a satellite imagery in the study. The RGB and NIR bands of Sentinel-2 and Landsat-9 were used for classification and comparison. LULC images were generated using pixel-based supervised Random Forest machine learning algorithms for classification. In this study, the study area was classified into four land classes, i.e. Forest, Agriculture, Settlements, and Waterbodies. As a result of the accuracy assessment, the Kappa statistics for Sentinel-2 and Landsat-9 data were 0.78 and 0.72 respectively. The resultsobtained showed that Sentinel-2 MSI presents more satisfying LULC images than Landsat-9 TOA data. However, this situation can change if different statistics and classification methods are used.

* *Corresponding author*
E-mail address: dhakalsandesh33@gmai.com
Received 11/6/2022 Accepted 2/1/2023

Introduction

Land cover refers to the observed physical cover on the earth's surface, whereas land use is characterized by the arrangements, activities, and inputs of people that impact, change or maintain land cover (FAO, 2016). Creating land use and land change (LULC) imagery has gained attention in recent years for sustainable land management, landscape ecology, and climate-related research (Carrasco et al., 2020). Additionally, knowledge of temporal changes in LULC gives us baseline information about planning, management, and sustainable use of natural resources (Paudel et al., 2016). Therefore, land use data is needed for the analysis of environmental processes and problems and improving or maintaining living conditions and standards. In particular, it is important to regularly track LULC changes in fast-growing regions where uncontrolled and irregular population expansion in cities can change urban climates.

Remote sensing is an evolving and powerful tool for assessing changes in land cover from small to larger spatial scales. Satellite imagery is one of the primary sources of information to analyse and retrieve LULC images. In particular, several algorithms have been developed and better accuracy obtained with advances in remote sensing technologies and sensor types (Carrasco et al., 2019). Recently launched Sentinel-2 MSI and Landsat-9 TOA satellites represent a new generation of Earth observation satellites. So, in this study, these satellite images were selected as data sources. Sentinel-2 data alone, Landsat-9 data alone, or both together, have been the data source for numerous studies, such as river bathymetry, monitoring inland water, land surface temperature, and water quality assessment (Niroumand-Jadidi et al., 2022a; Ye et al., 2022; Niroumand-Jadidi et al., 2022b). Various approaches, such as a comparison of machine learning classifiers, have been used to determine which method of data management produces more accurate findings (Bouslihim et al., 2022). This study uses Sentinel-2 MSI and Landsat-9 TOR data sets to generate an LULC map using the supervised Random Forest machine learning algorithm for the classification method. The main objective of this study is to compare and identify which of these two-satellite imagery performs with higher accuracy and applicability under similar conditions. Finally, we evaluate the overall accuracy, the Kappa coefficient, theuser accuracy, and the producer accuracy to determine and compare the results.

Materials and methods

Study area

The study area, Pokhara Metropolitan, is located in the hilly region of Nepal (Figure 1) between longitudes 83°48'E and 84°13'11"E and latitudes 28°4'39"N and 28°36'18"N. It is one of the largest cities in Nepal, with a total area of 465.01 square kilometres. Pokhara city is the capital of the Gandaki province, with many governmental offices located in the area. It is the focal point for the different districts of the Gandaki province for education, health, business, electricity, transportation, communication, and tourism. It is also an important industrial region in central Nepal. Due to rapid growth in population and several anthropogenic factors, the land cover and land use patterns of this city have been substantially modified and changed over the years. Therefore, to assist and promote better informed land use planning and decision-making, this study aims to create detailed information on land use and land cover. The study area was deliberately selected to represent ahilly region with rapid change in land cover and land use due to urbanization, internal migration, and infrastructural development. The area is familiar to the researchers and is feasible for field verification and validation of results.

Data collection

The composite imagery data sets from both Sentinel-2 MSI and Landsat-9 TOR, acquired

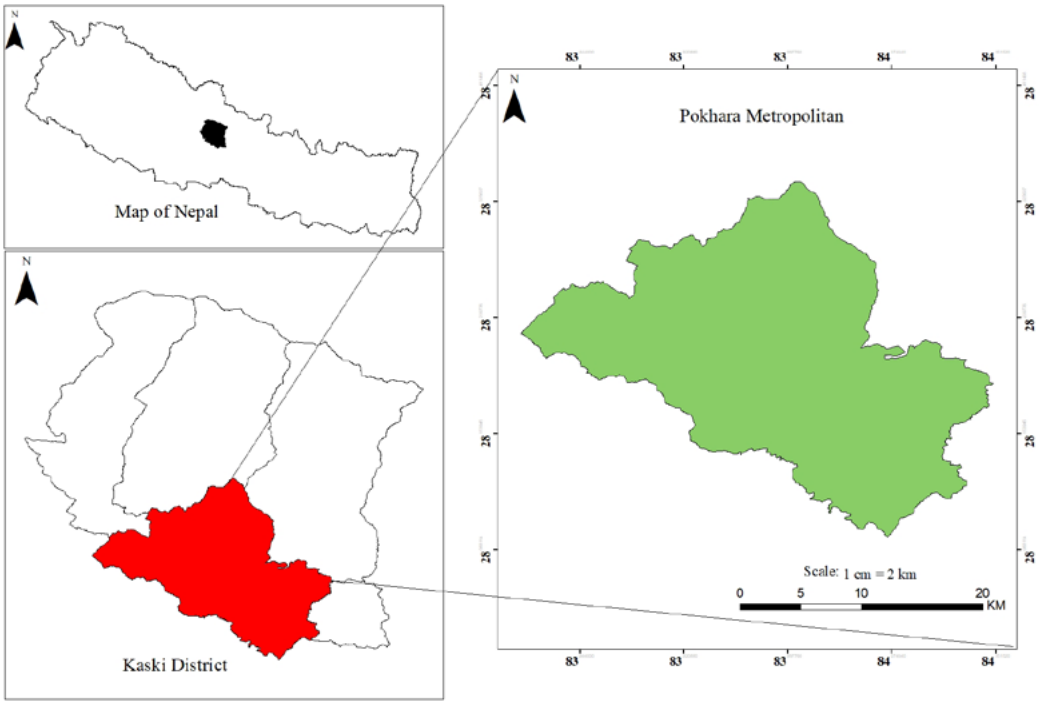

Figure 1: Map of the study area

for the period from January 1, 2022 to August 31, 2022, were gained for this study. Common bands of those two datasets, viz. Green (G), Red (R), Blue (B), and Near Infrared (NIR), were used in the classification process. Table 1 lists the spectral bands and ground sampling distance (GSD) values for both satellites.

Before the image classification process, pre-processing steps for satellite images were implemented. As there are multiple images

Table 1: Spectral bands and GSD value of data set

Landsat-9 Specifications			Sentinel-2 Specifications		
Bands	**Wavelength (µm)**	**GSD (m)**	**Bands**	**Central Wavelength**	**GSD (m)**
B1	0.43 - 0.45	30	B2	496.6nm (S2A) / 492.1nm (S2B)	10
B2	0.45 - 0.51	30	B3	560nm (S2A) / 559nm (S2B)	
B3	0.53 - 0.59	30	B4	664.5nm (S2A) / 665nm (S2B)	
B4	0.64 - 0.67	30	B8	835.1nm (S2A) / 833nm (S2B)	
B5	0.85 - 0.88	30	B5	703.9nm (S2A) / 703.8nm (S2B)	20
B6	1.57 - 1.65	30	B6	740.2nm (S2A) / 739.1nm (S2B)	
B7	2.11 - 2.29	30	B7	782.5nm (S2A) / 779.7nm (S2B)	
B8	0.52 - 0.90	15	B8A	864.8nm (S2A) / 864nm (S2B)	
B9	1.36 - 1.38	15	B11	1613.7nm (S2A) / 1610.4nm (S2B)	
B10	10.60 - 11.19	30	B12	2202.4nm (S2A) / 2185.7nm (S2B)	
B11	11.50 - 12.51	30	B1	443.9nm (S2A) / 442.3nm (S2B)	60
			B9	945nm (S2A) / 943.2nm (S2B)	
			B10	1373.5nm (S2A) / 1376.9nm (S2B)	

available for the same region over time, the time period of a year was select to consolidate the images into a single image of LULC change. Landsat-9 TOA (top-of-atmosphere) data available on GEE is orthorectified and corrected for solar angle (USGS TOA product guide). It was not possible to obtain continuous 16-day cloud-free time series data sets to enable wall-to-wall coverage for any part of the region. To overcome this limitation and to ensure cloud-free or near-cloud-free wall-to-all coverage, 8-month composites (depending on the cloudiness of the regions) were composed. The preparation of composite images goes through various steps that include selecting and pre-processing images, cloud masking, shadow masking, BRDF correction, topographic correction, and compositing. When all these steps have been completed, there is a composite image of Pokhara for the year 2022. This image was multiplied by 10000 to ensure minimum data loss when converting to an integer data type, which greatly reduced the storage space used by the composites. This was done by importing Landsat-9 collection 2 Tier 1 TOA reflectance imagery. Finally, sorting was undertaken for cloud cover and the least cloudy scene was extracted. The red, green, blue, and NIR bands of two data sets are common, and, thus, these four bands were considered for layer stacking. For Landsat-9 data, band 2, band 3, band 4, and band 5 were layer stacked and then clipped to include the study area. The same pre-processing steps were implemented for Sentinel-2 data.

In this case study, four general classes of LULC were used, viz. forests, agriculture, settlement areas, and water bodies. Training points were derived from visual inspection of recently captured (2021–2022) freely available Google Earth Image (high spectral resolution imagery) to identify features that were entirely made up of one of the four classes (forest, waterbodies, settlement area, and agriculture). To ensure that training data were representative of the classes in the study area, training data were captured from all corners of the Pokhara metropolitan area to capture 200 to 250 training points for each class. The same training samples were used for both data sets. For validation purposes, 60 validation points were randomly collected using GPS aid during field visits.

The Random Forest machine learning algorithm (RFM) is the most common classification method introduced in the literature (Dang et al., 2020) and uses the statistics for each class in each band as a normally distributed function. Additionally, RF classifiers often reach higher accuracy levels than other techniques such as maximum likelihood, single decision trees, and single-layer neural networks and can successfully handle high data dimensionality (Belgiu et al., 2016; Na et al., 2010). The Random Forest methodology uses a machine learning technique called bootstrapping and aggregated de-correlated random decision trees to classify a dataset using the mode of predictions from all the decision trees (Breiman, 2001). The optimal splitting of the nodes is achieved by reducing the correlation between the trees, which is done by selecting random subspaces from the given data (features) and using bootstrap aggregation (bagging) to construct an ensemble of decision trees. Random Forest classifiers also provide a quantitative measurement of the contribution of each variable to the classification output, which is useful in evaluating the importance of each variable. The optimised parameter values were selected by selecting the training samples, running the RF algorithm, and testing the classification output for overall precision, the producer and the user in the error matrix. In addition to obtaining high overall accuracy, the objective is to achieve a good balance between producer's accuracy (or the absence of errors of omission) and user's accuracy (or least errors of commissions).

Results

The classified Landsat-9 and Sentinel-2 images are presented in Figure 2. Due to the spatial resolution of the datasets, general classes, viz. forest, agriculture, settlement, and waterbodies, were considered LULC classes.

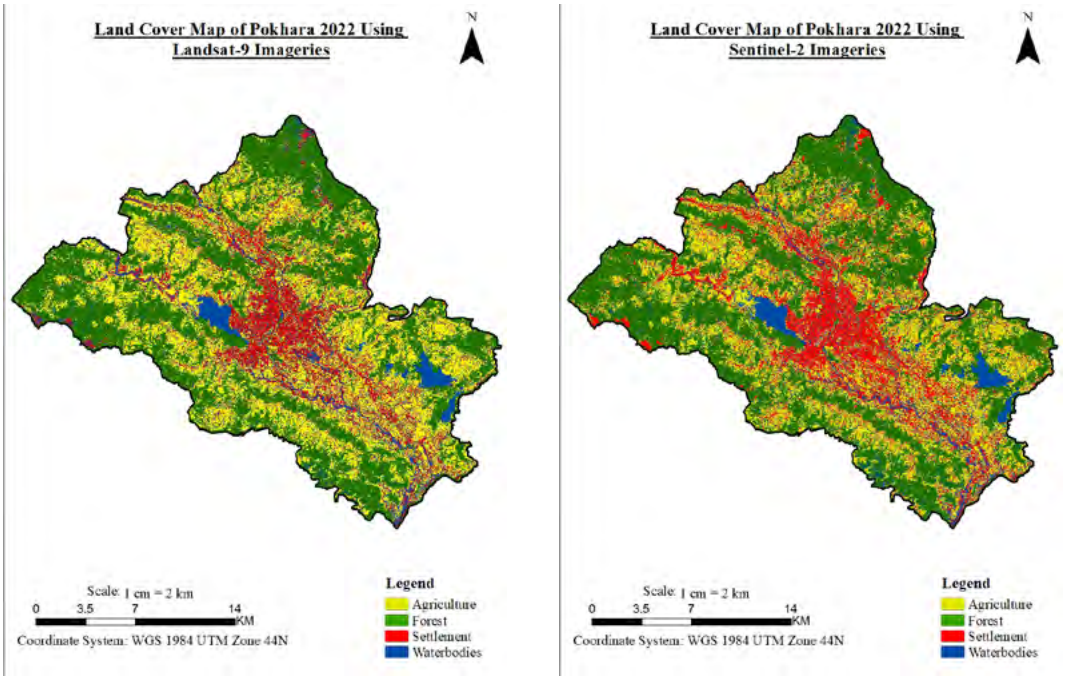

Figure 2: LULC image of the study area; A) Landsat-9 derived LULC, B) Sentinel-2 derived LULC

For LULC 2022, Landsat-9 and Sentinel-2 of the date 2022 were used. Random Forest classification was used for the classification of the image pre-processed. The results showed that forests were the main class of land cover, followed by agriculture, settlement, and water bodies (Table 2).

After generating LULC images, accuracy assessment validation points were collected with the aid of field visits using the Global Positioning System (GPS). In Table 3, an accuracy assessment report containing the accuracy of producers, the accuracy of users, the overall accuracy, and the Kappa coefficientis presented. As a result of the stratified random point evaluation, the Sentinel-2 derived LULC image had a Kappa value (0.78) and overall accuracy (83.70%), both of which were higher than that for the Landsat-9-derived LULC.This may be because Sentinel has a higher resolution as compared to Landsat, which provides more detailed information on smaller features (Ghayour et al., 2021). This is only a general evaluation, as these results can vary when using different statistics and classification methods for the accuracy assessment.

Discussion

In this study, we used common training data (common validation data) and the same

Table 2: Class-specific LULC of Pokhara Metropolitan in 2022

		LULC Landsat-9		LULC Sentinel-2	
S. N	Features	Area Km²	Percentage Cover	Area Km²	Percentage Cover
1	Forest	200.36	43.1%	194.89	41.9%
2	Waterbodies	48.86	10.5%	44.28	9.5%
3	Settlement	63.17	13.6%	75.83	16.3%
4	Agriculture	152.62	32.8%	150.01	32.3%
	Total	**465.01**	**100%**	**465.01**	**100%**

Table 3: Accuracy assessment result of LULC image

Land use Class	Landsat-9 LULC		Sentinel-2 LULC	
	UA	PA	UA	PA
Forest	82.5	86.84	89.47	100
Waterbodies	70	68.62	86	76.78
Settlement	80.55	74.35	70	82.35
Agriculture	86.36	90.47	88	81.48
Overall Accuracy	**79.41%**		**83.70%**	
KC	**0.72**		**0.78**	

UA= User's Accuracy, PA= Producer Accuracy, KC= Kappa Coefficient

machine learning algorithm to classify the Sentinel-2 and Landsat-9 images for LULC mapping. LULC was classified using the pixel-based supervised Random Forest machine learning algorithm, and the results were evaluated using the accuracy assessment by 60 random points. As a result of the accuracy assessment, the overall precision and Kappa coefficient for Landsat-9-derived LULC and Sentinel-2-derived LULC were 79.41%/0.72 and 83.70%/0.78 respectively. The resultant overall accuracy and Kappa coefficient showed that the Sentinel-2 LULC images best represent features with higher accuracy compared to the Landsat-9 LULC images.This supports asimilar finding by Bouslihim et al. (2022)using a machine learning classifier to compare pan-sharpened Landsat-9 and Sentinel-2 for land use classification. They found that, despite the improved resolution of pan-sharpened Landsat-9, Sentinel-2 images have significantly higher classification ability. Similarly, the results of our study indicate that Landsat-9 imagery classification shows slightly high waterbody coverage compared to Sentinel-2. The study conducted by Niroumand et al. (2022) to compare Landsat-9 and Sentinel-2 to retrieve water quality data also found that less grainy noise is visible in the Landsat-9 constituent maps, and matchup validation shows that Landsat-9 accuracy is generally higher in water quality mapping than Sentinel-2 (Niroumand-Jadidi et al., 2022b).This is because the increased signal-to-noise (SNR) and the greater dynamic range of OLI-2 are responsible for the enhanced Landsat-9 constituent.

Another study used S-2 and L-8 for the comparison of two composition methods, viz. seasonal composites and the percentile matrix using GEE (Xiao et al., 2022). Based on their result, S-2 exceeded L-8 spectral-temporal metrics at both class and overall levels, according to the accuracy evaluation results. The GEE platform is a powerful tool for analysinga wide variety of Landsat and Sentinel data simultaneously in one consolidated system. Basheer et al. compared the performance of different satellite datasets (i.e. Landsat, Sentinel, and Planet) and three classifiers, including support vector machine (SVM), maximum likelihood (ML), and random Forest (RF), to develop LULC (Basheer et al., 2022). According to their findings, S-2 produced higher accuracy than the L-8 datasets regardless of the classifier used. Similarly, in another study, Ahady et al. (2022) classified LULC from S-2 and L-8 using common training samples and created confusion matrixes using the same reference points for Sentinel-2 and Landsat-8 classification and comparison. Their findings show that overall accuracy was higher (94.26%) for Sentinel-2 while it was lower (85.04%) for Landsat-8. Similarly, it is the same for the Kappa coefficient. On the other hand, in the performance evaluation of various machine learning algorithms (SVM, ANN, MLC, MD, and MH) and in their comparison using S-2 and L-8 OLI data for LULC classification (Ghayour et al., 2021), Sentinel-2 data was slightly more accurate compared to Landsat-8. The results of this study are in line with those of the previous studies. Therefore, our work is another

illustration of the superior performance of Sentinel-2 compared to Landsat-9, using GEE.

Conclusion

The satellite images from Sentinel-2 and Landsat-9 were compared for the classification of the four classes, viz. forest, agriculture, settlements, and waterbodies, in Pokhara to see whichprovides the most accurate result. We used the same data range, the same training samples, the same number of points selected for each class, the same cloud masking percentage, the same classifier, and the same validation points for accuracy assessment of each image to compare the results. The result shows that the overall accuracy for the Sentinel-2-derived LULC is better than the Landsat-9-derived LULC. Therefore, this study concludes that Sentinel-2 images with the RFM algorithm for LULC preparation perform detailed land cover maps with better accuracy than Landsat-9 images, which is consistent with the findings of the previous studies. However, this situation may change if different classification and statistical techniques are applied.

REFERENCES

Ahady, A. B., & Kaplan, G. (2022). Classification comparison of Landsat-8 and Sentinel-2 data in Google Earth Engine, study case of the city of Kabul. *International Journal of Engineering and Geosciences*, *7*(1), 24-31. https://doi.org/10.26833/ijeg.860077

Basheer, S., Wang, X., Farooque, A. A., Nawaz, R. A., Liu, K., Adekanmbi, T., & Liu, S. (2022). Comparison of Land Use Land Cover Classifiers Using Different Satellite Imagery and Machine Learning Techniques. *Remote Sensing*, *14*(19). https://doi.org/10.3390/rs14194978

Belgiu, M., & Drăguţ, L. (2016). Random forest in remote sensing: A review of applications and future directions. *ISPRS Journal of Photogrammetry and Remote Sensing*, *114*, 24–31. https://doi.org/10.1016/j.isprsjprs.2016.01.011

Bouslihim, Y., Kharrou, M. H., Miftah, A., Attou, T., Bouchaou, L., & Chehbouni, A. (2022). Comparing Pan-sharpened Landsat-9 and Sentinel-2 for Land-Use Classification Using Machine Learning Classifiers. *Journal of Geovisualization and Spatial Analysis*, *6*(2), 35. https://doi.org/10.1007/s41651-022-00130-0

Breiman, L. (2001). Random Forests. *Machine Learning*, *45*(1), 5–32. https://doi.org/10.1023/A:1010933404324

Carrasco, L., O'Neil, A. W., Morton, R. D., & Rowland, C. S. (2019). Evaluating Combinations of Temporally Aggregated Sentinel-1, Sentinel-2 and Landsat 8 for Land Cover Mapping with Google Earth Engine. *Remote Sensing*, *11*(3). https://doi.org/10.3390/rs11030288

Carrasco, R. A., Pinheiro, M. M. F., Junior, J. M., Cicerelli, R. E., Silva, P. A., Osco, L. P., & Ramos, A. P. M. (2020). Land use/land cover change dynamics and their effects on land surface temperature in the western region of the state of São Paulo, Brazil. *Regional Environmental Change*, *20*(3), 96. https://doi.org/10.1007/s10113-020-01664-z

Dang, V.-H., Hoang, N.-D., Nguyen, L.-M.-D., Bui, D. T., & Samui, P. (2020). A Novel GIS-Based Random Forest Machine Algorithm for the Spatial Prediction of Shallow Landslide Susceptibility. *Forests*, *11*(1). https://doi.org/10.3390/f11010118

Di Gregorio, A. (2005). *Land cover classification system: Classification concepts and user manual: LCCS* (Vol. 2). Food & Agriculture Org.

Ghayour, L., Neshat, A., Paryani, S., Shahabi, H., Shirzadi, A., Chen, W., Al-Ansari, N., Geertsema, M., Pourmehdi Amiri, M., Gholamnia, M., Dou, J., & Ahmad, A. (2021). Performance Evaluation of Sentinel-2 and Landsat 8 OLI Data for Land Cover/Use Classification Using a Comparison between Machine Learning Algorithms. *Remote Sensing*, *13*(7). https://doi.org/10.3390/rs13071349

Na, X., Zhang, S., Li, X., Yu, H., & Liu, C. (2010). Improved land cover mapping using random forests combined with landsat thematic mapper imagery and ancillary geographic data. *PE&RS, Photogrammetric Engineering & Remote Sensing*, *76*(7), 833–840.

Nasiri, V., Deljouei, A., Moradi, F., Sadeghi, S. M. M., & Borz, S. A. (2022). Land Use and Land Cover Mapping Using Sentinel-2, Landsat-8 Satellite Images, and Google Earth Engine: A Comparison of Two Composition Methods. *Remote Sensing*, *14*(9). https://doi.org/10.3390/rs14091977

Niroumand-Jadidi, M., Bovolo, F., Bresciani, M.,

Gege, P., & Giardino, C. (2022). Water Quality Retrieval from Landsat-9 (OLI-2) Imagery and Comparison to Sentinel-2. *Remote Sensing*, *14*(18). https://doi.org/10.3390/rs14184596

Niroumand-Jadidi, M., Legleiter, C. J., & Bovolo, F. (2022). River Bathymetry Retrieval From Landsat-9 Images Based on Neural Networks and Comparison to SuperDove and Sentinel-2. *IEEE Journal of Selected Topics in Applied Earth Observations and Remote Sensing*, *15*, 5250–5260. https://doi.org/10.1109/JSTARS.2022.3187179

Paudel, B., Zhang, Y., Li, S., Liu, L., Wu, X., & Khanal, N. R. (2016). Review of studies on land use and land cover change in Nepal. *Journal of Mountain Science*, *13*(4), 643–660. https://doi.org/10.1007/s11629-015-3604-9

Ye, X., Ren, H., Zhu, J., Fan, W., & Qin, Q. (2022). Split-Window Algorithm for Land Surface Temperature Retrieval From Landsat-9 Remote Sensing Images. *IEEE Geoscience and Remote Sensing Letters*, *19*, 1–5. https://doi.org/10.1109/LGRS.2022.3184980